Optimizing active and passive calibration of optical tweezers

2011 J. Opt. 13 044020

(http://iopscience.iop.org/2040-8986/13/4/044020)

IOP Publishing Journal of Optics
J. Opt. **13** (2011) 044020 (6pp) doi:10.1088/2040-8978/13/4/044020

Optimizing active and passive calibration of optical tweezers

M Andersson[1,2], F Czerwinski[1] and L B Oddershede

The Niels Bohr Institute, University of Copenhagen, Blegdamsvej 17, 2100 Copenhagen, Denmark

E-mail: magnusan@nbi.dk, czerwinski@nbi.dk and oddershede@nbi.dk

Received 29 April 2010, accepted for publication 12 October 2010
Published 4 March 2011
Online at stacks.iop.org/JOpt/13/044020

Abstract
To obtain quantitative information from optical trapping experiments it is essential to perform a precise force calibration. Therefore, sources of noise should be pinpointed and eliminated. Fourier analysis is routinely used to calibrate optical trapping assays because it is excellent for pinpointing high frequency noise. In addition, Allan variance analysis is particularly useful for quantifying low frequency noise and for predicting the optimal measurement time. We show how to use Allan variance in combination with Fourier analysis for optimal calibration and noise reduction in optical trapping assays. The methods are applied to passive assays, utilizing the thermal motion of a trapped particle, and to active assays where the bead is harmonically driven. The active method must be applied in assays where, for example, the viscoelastic properties of the medium or the size or shape of the trapped object are unknown. For measurement times shorter than the optimal calibration time the noise is larger in active than in the passive assays. For times equal to or longer than the optimal measurement time, though, the noise on passive and active assays is identical. As an example, we show how to quantify the influence on measurement noise of bead size and chamber geometry in active and passive assays.

Keywords: optical tweezers, active calibration, passive calibration, Allan variance, power spectrum, noise, drift, laser

(Some figures in this article are in colour only in the electronic version)

1. Introduction

The possibility of performing precise micro-manipulation and measuring interactions and dynamic properties of single molecules has resulted in optical tweezers being a valuable technique in the field of biophysics [1]. To use optical tweezers in quantitative force studies, a bead, typically a polystyrene bead in the micrometer regime, is used as force transducer. To calculate the exact forces exerted on the bead it is crucial to perform force calibrations as precisely as possible. Calibration protocols for precise force and position determination typically involve either passive calibration, where the Brownian motion of the trapped particle is monitored, or active calibration where the measurement chamber is oscillated with respect to the trapped bead [2, 3]. Active calibration has the advantage of reducing the number of variables, for example neither the viscosity nor the size of the trapped object nor its distance to nearby surfaces need to be known [2, 4, 5]. The number of assumptions in the final calibration step can thereby be reduced. In addition, since the forces measured are in the sub-pN to hundreds of pN range, optical trapping assays are extremely sensitive to noise picked up by the instrumentation from the surrounding environment and to drift originating from laser instabilities and temperature gradients, for example. Clever modifications to the classical single beam optical trapping assay have been invoked to minimize the effect of drift and noise [6–10]. However, the impact of drift on active calibration protocols has not yet been systematically addressed and quantified.

Most high precision optical trapping assays routinely perform Fourier analysis of the trapped particle positions, which yield a power spectrum that can be used to deduce

[1] Authors contributed equally.
[2] Present address: Depart. of Physics, Umea University, 901 87 Umea, Sweden.

the spring constant, characterize the quality of the trap, and quantify high frequency noise [11]. However, Fourier analysis is not a very efficient method for pinpointing low frequency noise and determining the optimal measurement time for calibration, for example for single molecule assays. For this purpose, Allan variance has proven to be a better choice [12–14]. In previous studies, the effect of very low frequency noise sources present in typical passive assays was investigated, these include the noise dependence of detection frequency, the type of photodiode, presence of a passive piezo stage with capacitive feedback loop, and presence of acoustic noise [12]. Here, we focus on quantification of noise in active calibration assays. Also, we show how to routinely implement Allan variance analysis alongside power spectral analysis and provide an optimized protocol that will allow the user to improve the signal to noise ratio in both passive and active optical trapping assays. As an example of how to use this optimized method, we performed both active and passive Allan variance analysis of optically trapped beads of different sizes in different chamber geometries with the goal of quantifying the corresponding noise contribution and determining the optimal measurement time for both passive and active calibration assays.

2. Materials and methods

2.1. Sample preparation

Measurement chambers with different heights and width-to-length ratios were made from two 100 μm thick glass slides, with either a single layer of Parafilm 110 ± 5 μm or a double layer of Parafilm 220 ± 10 μm that were cut into different geometries and placed between the cover slides as spacers. Cover slides were mended by heating the flow cell to 80 °C. Air bubbles in the film were removed by gently applying pressure to the top slide. Open chambers were made in a similar manner to that described in [15]. Phosphate buffered saline (PBS, 1×) was filtered with a 50 nm pore sized Millipore filter and degassed in ultrasound for 5 min. The buffer was used to prepare dilutions of polystyrene microspheres (1:50 000 from stock) of nominal diameter 792 ± 23 nm and 2035 ± 45 nm (Polybead, Polysciences Inc.). The measurement chamber was sealed with nail polish to prevent evaporation and mounted on a piezo stage (Physics Instrument, P-517.3CL) operated in a closed loop. Experiments were conducted at room temperature, 23 °C.

2.2. Experimental procedures

The model system and technical approach used for studying noise in optical tweezers have been described in detail previously [12]. In short, optical tweezers were implemented in an inverted microscope (Leica, DMI 6000 B). The laser was a continuous-wave Nd:YVO_4 (Spectra Physics J20I-BL-106C) operated at 800 mW, of which approximately 20% reached the sample. The forward scattered laser light was collected on a position sensitive diode (Pacific Silicon Sensor, DL100-7PCBA3) in order to determine the position of the bead within the trap. To allow for trapping of beads deep within the chamber we used a water immersion objective (Leica, HCX, 63×, NA = 1.20). The height of the chamber was measured using the characteristic laser reflection from the two surfaces and a bead was subsequently trapped at 50 μm from the bottom surface to minimize the hydrodynamic interactions with the cover slides. The bead positions were measured for 12 min with the position sensitive photodiode. The acquisition frequency was 22 kHz. Furthermore, acquisition card settings were chosen to ensure the best possible data reliability. A schematic illustration of the experimental setting is shown in figure 1.

We performed both passive and active calibrations along the optimized protocol outlined in section 2.4. For the passive calibration we simply recorded the positions of the bead performing thermal motion within the trap. For the active measurements the piezo stage was driven in a sinusoidal motion at 8, 32, or 128 Hz with an amplitude of 300 nm. Piezo and bead positions were recorded for all measurements. The data were streamed to the computer utilizing a LabVIEW program optimized for reliable streaming of large time series [16]. After each measurement, both active and passive, the data were scrutinized to find the trapping stiffness by the power spectrum calibration procedure [11, 17] and the noise in the experiment was quantified using the Allan variance approach [12, 18, 19]. The Allan variance of each data set was calculated by a custom-written Matlab program available for download [20].

2.3. Allan variance

Allan variance was designed to extrapolate the drift of a system at infinity from finite measurements [18]. In contrast to the normal variance, Allan variance converges to a finite value for a broad range of typical noise sources found in biophysical experiments, such as purely stochastic white noise, shot noise, damped oscillations etc. Therefore, Allan variance has proven itself a valuable tool to quantify the stability and noise of optical tweezers [12, 19, 21]. It gives an exact quantification of the variance for neighboring measurement intervals of length τ. This allows for extrapolating the timescale at which the system is affected by high frequency noise, for example that originating from electronic components, as well as low frequency noise such as vibrations, temperature gradients, etc.

For a time series with N elements and a total measurement time $t_{\mathrm{acq}} = N/f_{\mathrm{acq}}$ the Allan variance is defined as

$$\sigma_x^2(\tau) = \tfrac{1}{2}\langle (x_{i+1} - x_i)^2 \rangle_\tau \qquad (1)$$

where x_i is the mean over a time interval $\tau = m/f_{\mathrm{acq}}$, m being the number of elements in the interval. $\langle \cdots \rangle$ denotes the average over all combinations of neighboring intervals. The convergence of the Allan variance results in a significant gain in resolution, especially for $\tau \gg \tau_{\mathrm{c}}$, where τ_{c} is the typical correlation time of a particle undergoing Brownian motion in a harmonic trap. For measurement times significantly longer than τ_{c}, drift that is intrinsically present in every experimental setup becomes dominant over the fluctuations. At this transition a minimum of the Allan variance occurs, the corresponding time being the optimal measurement time

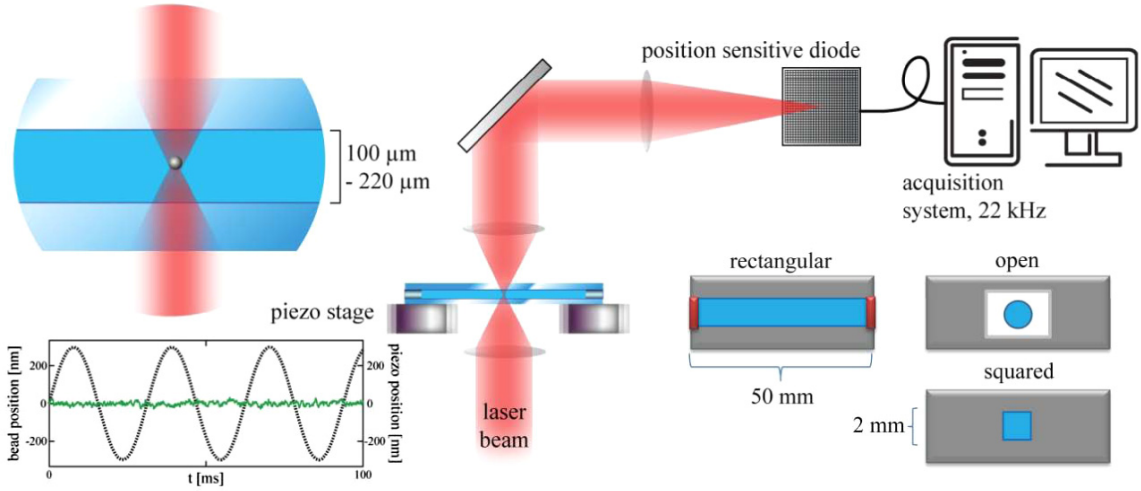

Figure 1. A schematic of the optical tweezers setup. A continuous Nd:YVO_4 laser operated at 800 mW was used to trap polystyrene beads 50 μm above the lower surface of the measurement chamber. The scattered light from the bead was imaged via the condenser onto a photodiode and digitized with custom-made LabVIEW software. The sample was mounted on a piezo stage, and during active calibration driven sinusoidally at 8, 32, and 128 Hz. Different measurement chamber geometries were tested.

for calibrations [12]. Allan variance is a direct measure of the accuracy and it is assumption free. It makes it possible to extrapolate the impact of typical low-frequency $1/f$-noise without the need to define bandwidth or filters. Since Fourier analysis lacks this quality, Allan variance and Fourier analysis probe complementary regimes of the frequency spectrum.

The thermal limit is given by the inherent uncertainty in determining the position of a bead with drag coefficient γ in a harmonic potential with spring constant k during the measurement time τ [12]:

$$\mathrm{SE}_{\langle x\rangle} = \sqrt{\frac{2k_\mathrm{B}T\gamma}{k^2\tau}}. \qquad (2)$$

If not oversampled, the Allan deviation cannot overcome this standard error. The closer the Allan deviation is to the thermal limit, the less noisy the trapping facility. For $\tau > 2\pi^2\tau_\mathrm{c}$ the Allan deviation follows the $-1/2$ scaling of the thermal limit with respect to τ.

2.4. Optimized protocol for calibration of optical tweezers setups

To quantitatively address and possibly minimize the noise present in an optical tweezers assay, we suggest an optimized protocol for optical trapping calibration that combines power spectral and Allan variance analysis:

(i) Sample position data in a passive calibration experiment for long time series with a sufficiently high acquisition frequency.
(ii) Calculate Allan variance of adjacent time series for a set of measurement times τ.
(iii) Determine optimal measurement time $\tau(\sigma_{x,\mathrm{min}})$ where the Allan deviation is minimal. Use this optimal measurement time for passive and active calibrations.
(iv) Calibrate over statistically independent intervals of length $\tau(\sigma_{x,\mathrm{min}})$ using the power spectral density method [11].
(v) If desirable, perform (i)–(iv) with active driving and fit power spectral density accordingly to [2]. This is particularly useful if the drag coefficient of the trapped object or the viscoelastic properties of the surrounding media are unknown [2, 3, 22].
(vi) Average the fitting parameters (corner frequency f_c, conversion factors relating output voltages to distance) of consecutive, statistically independent intervals.
(vii) Convert the Allan deviation from voltage units to meters, compare to the thermal limit.
(viii) Compare internal (e.g. active driving) and external noise (e.g. drift) levels. Quantify and possibly minimize noise sources.

This optimal protocol is not limited to optically trapped spherical particles, but is applicable to any kind of commonly used optical tweezers handles. For example, its use on gold nanorods and quantum dots has been demonstrated [13, 14].

3. Results

3.1. PSD in combination with Allan variance

Allan variance analysis can easily be performed together with the more conventional power spectral analysis, typically performed to find the force characteristics of the optical trap. To show how both power spectral density (PSD) and Allan variance can even be presented in the same plot, we used the data from a trapped 792 nm bead and sampled its position for 12 min. In figure 2, the corresponding power spectrum, averaged 4, 32, and 8192 times, respectively, is plotted together with the Allan variance of the same time sequence. To get the same physical values plotted on the ordinate axis for both the Allan variance and the PSD, the Allan variance was plotted as $2\tau\sigma_x^2$ as a function of $\pi\tau$, where $\pi\tau = f^{-1}$. The reason for the emergence of the factors π and 2 is due to the particular form of Fourier transformation used [11]. Interestingly, the

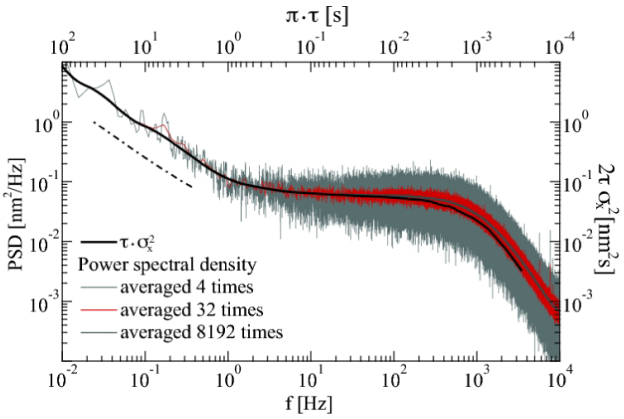

Figure 2. Power spectral density plots of a trapped bead averaged over 4, 32, and 8192 time series. Overlaid is the corresponding product of the Allan variance and measurement time (solid black line). The dashed–dotted line illustrates the typical $1/f$-slope for very low frequency noise.

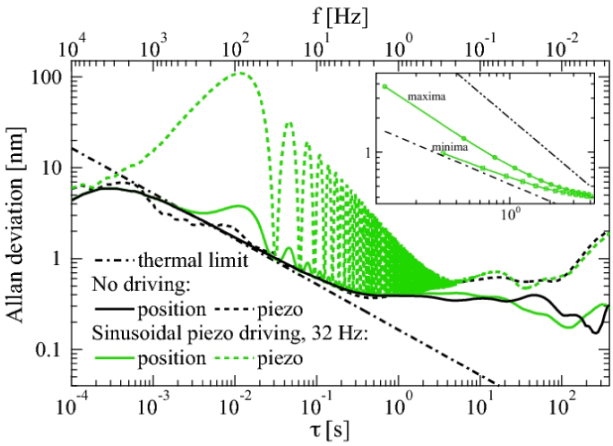

Figure 3. Allan deviation is plotted as a function of τ for passive (black lines) and active (32 Hz, green lines) calibrations. The solid lines show the Allan deviation of the positions of the bead, dashed lines show the Allan deviation of the output from the piezo stage. The dashed–dotted line denotes the thermal limit. The inset shows the minimum and maximum values of the deviation of the bead position during active calibration, shown along with the thermal limit and a guide-to-the-eye of slope -1.

Allan variance (solid black line) is able to reconstruct the power spectrum and yields a high resolution analysis of the data, particularly at low frequencies. Considerable averaging is needed to make the PSD equally precise as the Allan variance of the same dataset. The power spectrum yields noisier information for the low frequencies, hence details regarding noise and drift are lost. For high frequencies, the product of Allan variance and measurement time is slightly smaller than the power spectral density, due to the fact that Allan variance only considers neighboring intervals.

3.2. Active versus passive calibration

Active calibration has the advantage of needing less pre-knowledge about the system for which the force constant, for example, is sought. However, introducing an oscillatory motion could potentially increase the overall noise and influence the optimal measurement time. To investigate these issues we performed an experiment where a 792 nm bead was held by a stationary trap and the chamber was moved in a sinusoidal motion at 32 Hz. Also, we performed a passive calibration of the same bead. The resulting Allan deviation plots of the positions of the bead as well as the output from the piezo stage are shown in figure 3. The solid lines show the Allan deviation of the bead's positions and dashed lines denote the output from the piezo stage, which was turned on during both the active and passive experiments but kept stationary for the passive experiments. Green lines denote active calibration, black lines passive calibration. The dashed–dotted line denotes the thermal limit given by equation (2). It represents the lower limit for position detection. The trace of the passively calibrated particle (solid black line) shows that for low frequencies, noise levels are very close to the thermal limit, a benchmark of a stable setup. In accordance with previous results, the optimal measurement time is of the order of seconds, and for measurement times longer than tens of seconds the piezo stage, which was turned on but not moving, adds significant noise to the measurements [12]. For the active calibration, figure 3 can be divided into two distinct regions, one where the driven oscillation still dominates the motion of the bead, $\tau < 6$ s, and another for longer measurement times, $\tau > 6$ s, where the Allan deviations originating from passive and active calibrations, respectively, overlap completely. In this region drift dominates the measurement. Hence, our results show that active methods have a position accuracy that is equally as good as passive calibrations provided that the measurement time is long enough. The inset of figure 3 shows the maximum and minimum values of the positions of the bead during active calibration, when the piezo is run at 32 Hz (green symbols and lines). The maxima and minima converge and become indistinguishable for $\tau > 3$ s. Also shown are the thermal limit (dashed–dotted line) and a guide-to-the-eye of slope -1 (dashed–double-dotted line).

To zoom in on the optimal time measurement period for active calibration, we considered the divergence of the Allan deviation from the thermal limit for various driving frequencies (8, 32, and 128 Hz). Figure 4 shows the Allan deviations of a bead undergoing active calibration subtracted from the thermal limit. Fits with τ^{-1} scaling to the maximum peak values for each data set show that the deviation from the thermal limit rapidly decreases and they converge, with a deviation less than one 0.1 nm, already at approximately 1 s. The inset is a zoom in on the interesting region where the influence of the oscillations falls below the noise present from other external sources.

3.3. Variations in bead size and chamber geometry

As an example of how to go through the experimental settings with the aim of minimizing noise, we performed active and passive calibrations to pinpoint the effect of changing bead size and chamber geometry. Two different beads, with diameters of 792 and 2035 nm, were trapped with the same laser power and the frequency of the active calibration was 32 Hz. Instead of

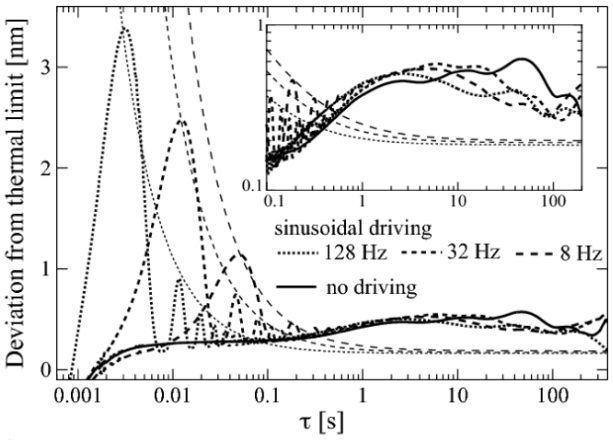

Figure 4. Difference between the Allan deviation of the position of a trapped bead during active calibration at 8, 32, and 128 Hz and the thermal limit. Fits to the maxima with τ^{-1}-scaling are also plotted. The inset is a zoom in on the interesting region where the drift begins to dominate the noise induced by the active calibration procedure.

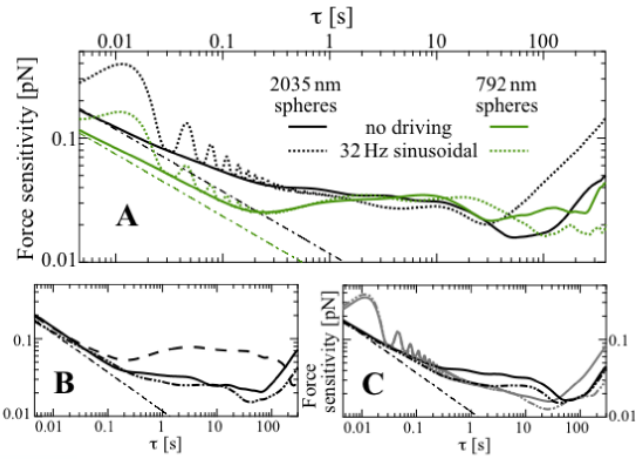

Figure 5. Application of Allan variance analysis to pinpoint noise sources in experimental settings. (A) Comparison of force sensitivity for beads with diameters of 792 nm (green lines) and 2035 nm (black lines) undergoing both passive (solid lines) and active (dotted lines) calibrations. (B) Force sensitivity for a bead trapped in a rectangular chamber 50 × 2 mm^2 (solid line), a quadratic chamber 2 × 2 mm^2 (dashed–double-dotted line), and open chamber (dashed line). (C) Comparison of the force sensitivity for chambers with a height of 100 μm (solid lines) and 200 μm (dashed–double-dotted lines) during active calibration (32 Hz, gray) and passive calibration (black). All dashed–dotted lines denote the thermal limit.

the usual Allan variance plots, for the noise analysis we chose to use the closely related force sensitivity $\Delta F = k(\sigma_x^2)^{1/2}$, with k being the spring constant characterizing the stiffness of the harmonic optical trapping potential. The force sensitivities as a function of τ are shown in figure 5(a), both for the smaller bead (green lines) and for the larger bead (black lines) undergoing passive (solid lines) or active (dotted lines) calibration. The thermal limits for the two bead sizes are shown with dashed–dotted lines. As is seen in the figure, the variation in force for short timescales $\tau < 1$ s is higher for the larger bead and the drift on the longer timescales also appears somewhat higher for the larger bead. Around the optimal measurement time (1 s $< \tau <$ 20 s) the noise contributions to the force are nearly identical for the two bead sizes.

To investigate the possibility of designing a low-noise chamber, we made systematic investigations of the force sensitivities of similar beads within a variety of chambers. In one series of experiments we systematically changed the aspect ratio in the lateral direction with respect to the trapping laser beam. Some results are shown in figure 5(b), where the force sensitivity is plotted versus τ for a quadratic chamber with lateral dimensions of 2 × 2 mm^2 (dashed–double-dotted line), a 2 × 50 mm^2 rectangular chamber (solid line), and a chamber where the circular droplet of bead solution did not touch the Parafilm (dashed line)—we denote this as an open chamber. The height of all three chamber types was 100 μm. The thermal limit is plotted by a dashed–dotted line in figure 5(b). Interestingly, we found that the aspect ratio of the chamber did not affect the noise level when the chamber was closed, i.e. the liquid was in contact with the Parafilm. The open chamber consistently picked up more noise, approximately 50 fN, in a 1–100 s timescale. Lastly, we investigated how varying the chamber height might affect the noise; figure 5(c) shows the force sensitivity as a function of τ for trapped 792 nm beads in chambers with heights of 100 μm (solid lines) and 200 μm (dashed–double-dotted lines). The beads underwent both passive (black lines) and active (gray lines) calibration. The effect of varying chamber height, doubling the volume, was minor, with regard to both the optimal measurement time and the absolute force sensitivity, though with a tendency for the shallower chamber to pick up more noise.

4. Discussion and conclusion

As Fourier analysis and Allan variance analysis have different strengths, the optimal strategy encompasses the use of both methods. It is convenient to have both present in the same representation, as shown in figure 2. Fourier analysis is especially efficient for pinpointing high frequency noise contributions, whereas Allan variance analysis elegantly quantifies low frequency contributions and provides the optimal measurement time, balancing the gain of drawing additional data points from a given distribution with the fact that inevitably for long enough timescales drift kicks in.

We systematically investigated the noise contribution from both passive and active calibrations, the latter involving a sinusoidal motion of the chamber with respect to the trapped bead. Active calibration procedures are often attractive, especially if, for example, the friction coefficient of the trapped particle or the viscosity of the medium [2] are unknown. If active methods are used in combination with passive methods, one can even deduce trapping properties in an unknown viscoelastic environment like the cytoplasm of a living cell [3, 22]. Due to the active driving, it is not surprising that at measurement times shorter than the optimal measurement time the noise on active assays is considerably larger than on passive assays. It was previously showed that the mere presence of a turned on but not actively moving piezo stage introduces significant noise to an optical

trapping assay [12]. Interestingly, our results showed that on timescales equal to or longer than the optimal measurement time, active calibration does not introduce additional noise in comparison to passive calibration. This is true for all driving frequencies tested (8–128 Hz). Therefore, the contribution of low frequency noise from the piezo stage might be linked to the feedback of the controller itself. However, care should be taken, since piezo stages have different inherent properties, for example resonance frequencies. A comparison of the maxima of the bead response in active calibration to the thermal limit in an Allan deviation graph allows for a good estimate of suitable driving frequencies and optimal measurement times.

The optimized active and passive calibration routine can be used to pinpoint noise in specific experimental settings. As an example, we investigated if the level of noise would be dependent on the bead size or chamber geometry. For both short and long times the smaller beads picked up less noise than the larger beads, but the noise levels for large and small beads were identical in the optimal measurement time interval. These conclusions are valid for both active and passive calibration. The noise picked up by a bead in chambers where we systematically varied the lateral aspect ratio and the height of the chamber did not depend on the chamber geometry. However, a bead in an open chamber picked up significantly more noise than in a closed chamber. Hence, to minimize noise we would recommend using closed chambers.

Every experimental setup and its environmental conditions are slightly different. By employing a combination of power spectral analysis and Allan variance analysis and reporting the outcomes to systematic changes, noise sources can be found, quantified and sometimes eliminated. Implementing these routines on a daily basis holds the potential to compare various setups and measurements across different laboratories with the goal of improving optical trapping standards.

Acknowledgments

We acknowledge useful discussions with Joanne L Gornall, Liselotte Jauffred, Ulrich F Keyser, and Oliver Otto and thank Nicola Girotti for help with illustrations. MA acknowledges financial support from the Swedish Research Council and LBO acknowledges support from the KU excellence program.

References

[1] Svoboda K and Block S M 1994 Biological applications of optical forces *Annu. Rev. Biophys. Biomol. Struct.* **23** 247–85

[2] Tolic-Nørrelykke S F, Schäffer E, Howard J, Pavone F S, Jülicher F and Flyvbjerg H 2006 Calibration of optical tweezers with positional detection in the back focal plane *Rev. Sci. Instrum.* **77** 103101

[3] Fischer M and Berg-Sorensen K 2007 Calibration of trapping force and response function of optical tweezers in viscoelastic media *J. Opt. A: Pure Appl. Opt.* **9** S239–50

[4] Deng Y, Bechhoefer J and Forde N R 2007 Brownian motion in a modulated optical trap *J. Opt. A: Pure Appl. Opt.* **9** S256–63

[5] Schäffer E, Nørrelykke S F and Howard J 2007 Surface forces and drag coefficients of microspheres near a plane surface measured with optical tweezers *Langmuir* **23** 3654–65

[6] Atakhorrami M, Addas K M and Schmidt C F 2008 Twin optical traps for two-particle cross-correlation measurements: eliminating cross-talk *Rev. Sci. Instrum.* **79** 043103

[7] Klein M, Andersson M, Axner O and Fällman E 2007 Dual-trap technique for reduction of low-frequency noise in force measuring optical tweezers *Appl. Opt.* **46** 405–12

[8] Abbondanzieri E A, Greenleaf W J, Shaevitz J W, Landick R and Block S M 2005 Direct observation of base-pair stepping by RNA polymerase *Nature* **438** 460–5

[9] Carter A R, Seol Y and Perkins T T 2009 Precision surface-coupled optical-trapping assay with one-basepair resolution *Biophys. J.* **96** 2926–34

[10] Wang M D, Schnitzer M J, Yin H, Landick R, Gelles J and Block S M 1998 Force and velocity measured for single molecules of RNA polymerase *Science* **282** 902–7

[11] Berg-Sørensen K and Flyvbjerg H 2004 Power spectrum analysis for optical tweezers *Rev. Sci. Instrum.* **75** 594–612

[12] Czerwinski F, Richardson A C and Oddershede L B 2009 Quantifying noise in optical tweezers by Allan variance *Opt. Express* **17** 13255–69

[13] Jauffred L, Sletmoen M, Czerwinski F and Oddershede L B 2010 Quantum dots as handles for optical manipulation *Proc. SPIE* **7762** 77620Q

[14] Czerwinski F, Richardson A C, Selhuber-Unkel C and Oddershede L B 2009 Quantifying and pinpointing sources of noise in optical tweezers experiments *Proc. SPIE* **7400** 740004

[15] Fällman E, Schedin S, Jass J, Andersson M, Uhlin B E and Axner O 2004 Optical tweezers based force measurement system for quantitating binding interactions: system design and application for the study of bacterial adhesion *Biosens. Bioelectron.* **19** 1429–37

[16] Czerwinski F and Oddershede L 2010 TimeSeriesStreaming.vi: LabView program for reliable data streaming of large analog time series *Comput. Phys. Commun.* doi:10.1016/j.cpc.2010/10.019
Czerwinski F and Oddershede L 2010 arXiv:1008.1413

[17] Hansen P M, Tolic-Nørrelykke I M, Flyvbjerg H and Berg-Sørensen K 2006 Tweezercalib 2.1: faster version of MatLab package for precise calibration of optical tweezers *Comput. Phys. Commun.* **175** 572–3

[18] Allan D W 1966 Statistics of atomic frequency standards *Proc. IEEE* **54** 221–30

[19] Gibson G M, Leach J, Keen S, Wright A J and Padgett M J 2008 Measuring the accuracy of particle position and force in optical tweezers using high-speed video microscopy *Opt. Express* **16** 14561–70

[20] Czerwinski F 2010 *Allan v3.0* MatlabCentral 26659 http://www.mathworks.com/matlabcentral/fileexchange/26659-allan-v3-0

[21] Mahamdeh M and Schäffer E 2009 Optical tweezers with millikelvin precision of temperature-controlled objectives and base-pair resolution *Opt. Express* **17** 17190–9

[22] Fischer M, Richardson A C, Reihani S N S, Oddershede L B and Berg-Sørensen K 2010 Active–passive calibration of optical tweezers in viscoelastic media *Rev. Sci. Instrum.* **81** 015103